Contributions of residential coal combustion to the air quality in Beijing-Tianjin-Hebei (BTH), China: A case study

Xia Li[1,2], Jiarui Wu[1], Miriam Elser[3], Tian Feng[1], Junji Cao[1], Imad El-Haddad[3], Rujin Huang[1], Xuexi Tie[3], André S. H. Prévôt[3], and Guohui Li[1*]

[1]Key Lab of Aerosol Chemistry and Physics, SKLLQG, Institute of Earth Environment, Chinese Academy of Sciences, Xi'an, China
[2]University of Chinese Academy of Science, Beijing, China
[3]Laboratory of Atmospheric Chemistry, Paul Scherrer Institute, 5232 Villigen, Switzerland

[*]Correspondence to: Guohui Li (ligh@ieecas.cn)

Abstract: In the present study, the WRF-Chem model is used to assess contributions of residential coal combustion (RCC) emission to the air quality in Beijing-Tianjin-Hebei (BTH) during a persistent air pollution episode from 9 to 25 January 2014. In general, the predicted temporal variations and spatial distributions of the mass concentrations of air pollutants are in good agreements with observations at monitoring sites in BTH. The WRF-Chem model also reasonably reproduces the temporal variations of aerosol species when compared with the AMS measurements in Beijing. The RCC emission plays an important role in the haze formation in BTH, contributing about 23.1% of $PM_{2.5}$ (fine particulate matter) and 42.6% of SO_2 during the simulation period on average. Organic aerosols dominate the $PM_{2.5}$ from the RCC emission in BTH, with a contribution of 42.8%, followed by sulfate (17.1%). The air quality in Beijing is remarkably improved when the RCC emission in BTH and its surrounding areas is excluded in model simulations, with a 30% decrease of $PM_{2.5}$ mass concentrations. However, if only the RCC emission in Beijing is excluded, the local $PM_{2.5}$ mass concentration is decreased by 18.0% on average. Our results suggest that the implementation of the residential coal replacement by clean energy sources in Beijing is beneficial to the local air quality. Should the residential coal replacement be carried out in BTH and its surrounding areas, the air quality in Beijing would be improved remarkably. Further studies would need to consider uncertainties in the emission inventory and meteorological fields.

41

42 ## 1 Introduction

43 Over the several past decades, China has experienced rapid economic growth,
44 accompanied with accelerating industrialization and urbanization, which has seriously
45 deteriorated air quality (e.g., Zhang et al., 2009; Zhang et al., 2012; Zhang et al., 2015).
46 Recently, haze pollution has become the primary concern about air quality in most key regions
47 and cities in China, especially in Beijing-Tianjin-Hebei (BTH) and Yangtze River Delta (YRD)
48 (e.g., Wang et al., 2005; An et al., 2007; Wang et al., 2014; Chen et al., 2016; Gao et al., 2016).
49 The severe and persistent haze pollution with high concentrations of fine particulate matter
50 ($PM_{2.5}$) and the consequent low visibility, is mainly caused by heavy anthropogenic emissions
51 and unfavorable synoptic situations (e.g., Seinfeld and Pandis, 2006; Lei et al., 2011; Lv et al.,
52 2016; Wang et al., 2016; Zíková et al., 2016). According to the China's Ministry of
53 Environment Protection (MEP), the annual mean mass concentration of $PM_{2.5}$ was 102 μg m^{-3}
54 in 2013 and 93 μg m^{-3} in 2014 in BTH, far beyond the World Health Organization (WHO)
55 interim target-1 of 35 μg m^{-3} for the annual mean $PM_{2.5}$ mass concentration and the secondary
56 class standard in China's new National Ambient Air Quality Standard (NAAQS, GB3095-
57 2012). Therefore, in order to improve the air quality in BTH, the Chinese State Council has
58 issued the "Atmospheric Pollution Prevention and Control Action Plan" (APPCAP) in
59 September 2013 to reduce $PM_{2.5}$ by 25% by 2017 relative to 2012 levels. Since implementation
60 of the APPCAP, stringent control strategies have been carried out to reduce pollutants
61 emissions from power plants, industries and transportation (Sheehan et al., 2014; Liu et al.,
62 2015; Yang et al., 2016). Control strategies have also been implemented to reduce residential
63 emissions, but evaluation means constrained by observations are still lacking.

64 The air pollution in China is a typical coal-smoke pollution, which is considered to be
65 closely associated with China's special energy consumption structure (e.g., Quan et al., 2014;
66 Archernicholls et al., 2016; Liu et al., 2016; Xue et al., 2016). Coal plays a key role in China's

energy structure, and as the most abundant and a relatively cheap energy resource, coal is regarded as a dominant energy supply in China in the foreseeable future. According to the BP statistical review of world energy, from 1980s to the present day, the proportion of coal in China' primary energy production and consumption has been around 70%, which is much higher than that of around 20% in OECD (Organization for Economic Co-operation and Development) countries. Entering the 21 centuries, coal consumption in China has increased sharply, and by 2013, China's coal consumption has accounted for 50.3% of the global coal consumption, which was 4.2 and 6.7 times higher than that of the United States and European Union, respectively. It is reported that in 2013, coal is responsible for 79%, 54%, 40%, 35%, 40%, and 17% of the SO_2, NO_x, PM_{10}, $PM_{2.5}$, BC, and OC emissions in China, respectively (Ma et al., 2016).

Residential coal combustion (RCC) emission is recognized as a significant source of air pollution, affecting both local and regional air quality and posing serious threat to human health and environment by releasing hazardous air pollutants, including particulate matter (PM), black carbon (BC), organic carbon (OC), SO_2, nitrogen oxide (NO_x), CO, CO_2, and polycyclic aromatic hydrocarbons (e.g., Wornat et al., 2001; Ge et al., 2004; Zhi et al., 2008; Shen et al., 2010; Cheng et al., 2016; Li et al., 2016). Recently, chemical transport models have been used to investigate the contribution of RCC emissions to the ambient air pollution in China. Using the CMAQ model, Xue et al. (2016) have shown that during the winter heating season of 2012, the contribution of RCC emissions in Beijing to the mass concentrations of local PM_{10}, SO_2, NO_x, and CO is 11.6%, 27.5%, 2.8%, and 7.3%, respectively. Simulations using the GEOS-Chem model by Ma et al. (2016) have demonstrated that coal combustion contributes 40% of the total $PM_{2.5}$ mass concentrations on national average in 2013. Among major coal-burning sectors, industrial coal burning contributes 17% of the $PM_{2.5}$ concentrations, followed by power plants (9.8%) and domestic sector (4.0%). Liu et al. (2016) have used the Weather Research

and Forecasting model coupled with chemistry (WRF-Chem) to simulate the air pollution in BTH in January and February 2010, indicating that annual elimination of residential sources in BTH reduces emissions of primary $PM_{2.5}$ by 32%, compared with 5%, 6%, and 58% of transportation, power plants, and industrial sectors, respectively. Using the source-oriented CMAQ model, Qiao et al. (2017) have conducted simulations to evaluate source apportionment of $PM_{2.5}$ in 25 Chinese provincial capitals and municipalities and concluded that industrial and residential sources are predicted to be the largest contributor to $PM_{2.5}$ for all the city groups, with annual fractional contributions of 25.0%-38.6% and 9.6%-27%, respectively.

Until now, there have been few studies focusing specially on the impacts of RCC emissions on the air quality in BTH. In the present study, we use the WRF-Chem model to assess the contribution of RCC emissions to the air quality in BTH during a persistent air pollution episode from 9 to 25 January 2014. The WRF-Chem model configurations and methodology are described in Section 2. Model results and discussions are represented in Section 3, and conclusions are given in Section 4.

2 Model and Methodology

2.1 WRF-Chem model and configurations

The WRF-Chem model used in this study is developed by Li et al. (2010, 2011a, b, 2012) at the Molina Center of Energy and Environment, based on previous studies (Grell et al., 2005; Fast et al., 2006). The wet deposition of aerosols follows the method used in the CMAQ module and the dry deposition of chemical species is parameterized following Wesely (1989). The photolysis rates are calculated using the FTUV (fast radiation transfer model), including the aerosol and cloud effects on photolysis (Tie et al., 2003; Li et al., 2005, 2011a). The inorganic aerosols are calculated using ISORROPIA Version 1.7 (Nenes, 1998). The secondary organic aerosol (SOA) is predicted using the volatility basis-set (VBS) modeling method, with

contributions from glyoxal and methylglyoxal.

The WRF-Chem model adopts one grid with a horizontal resolution of 6 km centered at 39°N, 117°E, and 35 sigma vertical levels with a stretched vertical grid with spacing ranging from 30 m near the surface, to 500 m at 2.5 km and 1 km above 14 km, and the grid cells used for the domain are 150 × 150. The physical parameterizations employed in the simulation include the microphysics scheme of Hong and Lim (2006), the unified Noah Land-surface model (Chen and Dudhia, 2001), the Goddard longwave scheme (Chou and Suarez, 2001), and the Goddard shortwave scheme (Chou and Suarez, 1999). The National Centers for Environmental Prediction (NCEP) 1°×1° reanalysis data are used for the meteorological initial and boundary conditions, and the meteorological simulations are not nudged in the study. The chemical initial and boundary conditions are interpolated from the 6 h output of MOZART (Horowitz et al., 2003). The spin-up time of the WRF-Chem model is 28 h. The monthly average anthropogenic emissions with a 6 km horizontal resolution in the North China Plain are developed by Zhang et al. (2009) with the base year of 2013, including contributions from agriculture, industry, power generation, residential, and transportation sources, and the volatile organic compounds (VOCs) speciation based on the SAPRC99 chemical mechanism. The temporal allocation for different sources follows those in Zhang et al. (2009). The biogenic emissions are calculated online using the MEGAN (Model of Emissions of Gases and Aerosol from Nature) model developed by Guenther et al. (2006).

A persistent air pollution episode from 9 to 25 in January 2014 in BTH is simulated using the WRF-Chem model. During the study period, the average $PM_{2.5}$ mass concentration in BTH is 161.9 μg m^{-3}, with a maximum of 323.5 μg m^{-3}. The average temperature and relative humidity in Beijing during the period is −1.7 ℃ and 32.3%, respectively, and the average wind speed is about 2.8 m s^{-1}. The model simulation domain is shown in Figure 1, and detailed model configurations can be found in Table 1.

The brute force method is used to quantify the contribution of the RCC emission in BTH and its surrounding areas to the air quality (Dunker et al., 1996). It is worth noting that, although the method can evaluate the importance of the certain emission source, it still has flaws in quantifying the source contribution, considering the complicated non-linear processes in the atmosphere (Zhang and Ying, 2011). In the present study, we have conducted one reference simulation in which emissions from various anthropogenic and biogenic sources are considered (hereafter referred as to the REF case). The results from the REF case are compared with observations in BTH to validate the model performance. Additional two sensitivity simulations have also been performed, without the RCC emission in BTH and its surrounding areas and Beijing, respectively (hereafter referred as to the SEN-BTH case and SEN-PEK case). In the sensitivity simulation, the emission of NO_x, CO, VOCs, SO_2, black and organic carbon, primary sulfate, and unspecified particulate matters from the RCC is turned off. The difference between the reference and sensitivity simulation is used to evaluate contributions of RCC emissions to the air quality in BTH and Beijing.

2.2 Statistical methods for comparisons

In the present study, we use the mean bias (MB), root mean square error (RMSE) and index of agreement (IOA) to validate the WRF-Chem model performance in simulating air pollutants and aerosol species against observations and measurements. IOA describes the relative difference between the model predictions and observations, ranging from 0 to 1, with 1 indicating perfect agreement of predictions and observations.

$$MB = \frac{1}{N}\sum_{i=1}^{N}(P_i - O_i)$$

$$RMSE = \left[\frac{1}{N}\sum_{i=1}^{N}(P_i - O_i)^2\right]^{\frac{1}{2}}$$

$$IOA = 1 - \frac{\sum_{i=1}^{N}(P_i - O_i)^2}{\sum_{i=1}^{N}(|P_i - \bar{O}| + |O_i - \bar{O}|)^2}$$

Where P_i and O_i are the predicted and observed mass concentrations of pollutants,

166 respectively. N is the total number of the predictions used for comparisons, and $\overline{P}$ and $\overline{O}$
167 represent the average of predictions and observations, respectively.

168 **2.3 Pollutants measurements**

169 The hourly near-surface CO, SO_2, NO_2, O_3, and $PM_{2.5}$ mass concentrations released by the
170 China's Ministry of Environmental Protection can be downloaded from the website
171 http://www.aqistudy.cn/. The sulfate, nitrate, ammonium, and organic aerosols (OA) have been
172 measured by the Aerodyne High Resolution Time-of-Flight Aerosol Mass Spectrometer (HR-
173 ToF-AMS) with a novel $PM_{2.5}$ lens from 9 to 26 January 2014 at the Institute of Remote
174 Sensing and Digital Earth (IRSDE), Chinese Academy of Sciences (40.00°N, 116.38°E) in
175 Beijing (Fig. 1) (Williams et al., 2013). The Positive Matrix Factorization (PMF) technique is
176 used with constraints implemented in SoFi (Canonaco et al., 2013) to analyze the sources of
177 OA and five components are separated by their mass spectra and time series. The components
178 include hydrocarbon-like OA (HOA), cooking OA (COA), biomass burning OA (BBOA), coal
179 combustion OA (CCOA), and oxygenated OA (OOA). HOA, COA, BBOA, and CCOA are
180 interpreted for surrogates of primary OA (POA), and OOA is a surrogate for SOA. Detailed
181 information about the HR-ToF-AMS measurements and data analysis can be found in Elser et
182 al. (2016).

183

184 **3 Results and discussions**

185 **3.1 Model performance**

186 **3.1.1 Air pollution simulations in BTH**

187 Considering the key role of meteorological fields in determining the formation
188 transformation, diffusion, transport, and removal of the air pollutants, Figure 2 presents the
189 diurnal profiles of the observed and simulated temperature, relative humidity (RH), wind speed
190 and direction at meteorological sites in Beijing, Tianjin, and Shijiazhuang during the simulation

period. The WRF-Chem model reasonably well predicts the diurnal variations of the temperature in the three cities against observations, with IOAs of around 0.80. The model also well yields the temporal variation of the RH in Beijing when compared with observations, but it tends to underestimate the RH in Tianjin and Shijiazhuang with IOAs less than 0.70, and generally fails to capture the high RH exceeding 80%. The temporal variations of the wind speed and direction in BTH are also reasonably reproduced, but the model biases are still rather large.

Figure 3 presents the distributions of predicted and observed near-surface mass concentrations of $PM_{2.5}$, O_3, NO_2, and SO_2 along with the simulated wind fields averaged from 9 to 25 January 2014 in BTH. Generally, the predicted spatial pattern of $PM_{2.5}$ is well consistent with observations at ambient monitoring sites in BTH. The WRF-Chem model reasonably reproduces the high $PM_{2.5}$ concentrations exceeding 150 μg m^{-3} in the plain region of BTH. Apparently, during the simulation period, the weak winds in the plain region of BTH facilitate the accumulation of $PM_{2.5}$, causing severe air pollution. The average simulated $PM_{2.5}$ mass concentrations exceed 250 μg m^{-3} in south Hebei, which is generally in good agreement with observations. The observed and simulated O_3 concentrations are rather low in the plain region of BTH with the high $PM_{2.5}$ level, varying from 10 to 30 μg m^{-3}. There are several reasons for the low O_3 concentrations in the plain region of BTH. Firstly, during wintertime, the insolation is weak in north China, which is unfavorable for the O_3 photochemical production. Additionally, high $PM_{2.5}$ concentrations and frequent occurrence of clouds during haze days further attenuate the incoming solar radiation in the planetary boundary layer (PBL), decreasing the O_3 levels. Secondly, weak winds indicate stagnant situations, lacking the O_3 transport from outside BTH. Thirdly, high NO_x emissions cause titration of O_3, which is shown by the high NO_2 concentrations in the plain region of BTH. The elevated NO_2 and SO_2 concentrations are observed and simulated in the plain region of BTH, particularly in cities and their surrounding

areas, ranging from 50 to 100 μg m^{-3} and 50 to 150 μg m^{-3}, respectively. It is worth noting that the simulated NO_2 is generally distributed evenly in the plain region of BTH, indicating the dominant contribution of area sources.

Figure 4 presents the diurnal profiles of observed and simulated near-surface $PM_{2.5}$, O_3, NO_2, SO_2, and CO mass concentrations averaged over all monitoring sites in BTH from 9 to 25 January 2014. The WRF-Chem model reproduces the diurnal variations of $PM_{2.5}$ mass concentrations when compared with observations in BTH during the simulation period. The MB and RMSE are only -2.7 and 40.9 μg m^{-3}, respectively, and the IOA is 0.94. During the persistent haze episode in BTH, the model generally well replicates the haze developing stage, but tends to underestimate the $PM_{2.5}$ concentrations against observations during the haze dissipation stage. One of the most possible reasons is the uncertainty of the simulated meteorological fields, which determine the formation, transformation, diffusion, transport, and removal of air pollutants in atmosphere (Bei et al., 2012, 2013). Should the predicted winds be intensified earlier than observations in BTH during the haze dissipation stage, the simulated $PM_{2.5}$ concentrations would decline earlier, causing the model underestimation. The predicted NO_2 diurnal variations are generally well consistent with observations, with a MB of 4.2 μg m^{-3} and an IOA of 0.93. The model also yields reasonable predictions for SO_2 and CO temporal variations with IOAs exceeding 0.85. However, the RMSE for SO_2 is rather large, showing considerable deviations of the SO_2 simulations. A large fraction of SO_2 are emitted from power plants or agglomerated industrial zones, which can be regarded as point sources, so the transport of SO_2 is more sensitive to uncertainties in simulated wind fields. The early occurrence of intensified winds in simulations also cause rapid falloff of SO_2 and CO mass concentrations during the haze dissipation stage. Besides uncertainties in meteorological field simulations, uncertainties in emission inventory are also responsible for the model biases of air pollutants. Since implementation of the APPCAP, strict emission control measures have been

made to improve the air quality in BTH, and the spatiotemporal variations of anthropogenic emissions in BTH have changed considerably (Li et al., 2017), which is not reflected in the emission inventory used in the present study.

Recently, observational studies have used CO as an aerosol proxy to investigate atmospheric aerosols based on the remote sensing technique. Figure 5 shows the scatter plots of observed and simulated $PM_{2.5}$ with CO mass concentrations averaged over all ambient monitoring sites in BTH during the simulation period. The observed and simulated CO mass concentrations are well correlated with those of $PM_{2.5}$, with the R^2 exceeding 0.81.

Table 2 presents the further validation of WRF-Chem model simulations of air pollutants based on statistics methods suggested by previous studies (US EPA, 2005; Boylan and Russell, 2006; Emery et al., 2017). Compared to the suggested model performance criteria of air pollutants, the WRF-Chem model performs well in simulating the air pollutants and aerosol species in this study. The FB, FE, NMB, and NME of $PM_{2.5}$ and O_3 are generally within the benchmarks, with the correlation coefficients approaching 0.90, showing good consistency between the simulations and observations. As for the aerosol species, except for sulfate, the differences between the observed and simulated organic aerosol, nitrate, and ammonium are all less than the reference criteria. The FB and FE of sulfate are reasonable, but the NMB of 37.6% and NME of 67.8% are slightly higher than the suggested criteria.

3.1.2 Aerosol species simulations in Beijing

Figure 6 presents the temporal profiles of measured and simulated OA, CCOA, sulfate, nitrate, and ammonium mass concentrations at IRSDE site in Beijing from 9 to 25 January 2014. The model generally performs reasonably well in simulating the diurnal variations of aerosol species when compared with the HR-ToF-AMS measurements, with IOAs exceeding 0.80. As a primary species, OA is primarily determined by direct emissions from various sources, including vehicles, cooking, biomass burning, coal combustion, and transport from

outside Beijing. Therefore, uncertainties in anthropogenic emissions and the simulated meteorological fields markedly influence the OA simulations (Bei et al., 2017). Although the IOA for OA is 0.84, the model slightly overestimates the OA mass concentrations with a MB of 5.1 μg m^{-3}, and the deviation of OA simulations is also large, with a RMSE of 42.3 μg m^{-3}. In addition, the model fails to reproduce the measured OA peaks during the nighttime on 11 and 17 January 2014, which is perhaps caused by the emission uncertainties. The model also generally tracks the measured diurnal variations of CCOA mass concentrations, with an IOA of 0.81. The model frequently underestimates or overestimates the CCOA mass concentrations and is also subject to missing the observed CCOA peaks. The CCOA is mainly emitted from industries and residential coal combustion. In general, the CCOA emissions from industries have clear diurnal variations, but are opposite for those from residential coal combustion, causing large model biases for the CCOA simulation. The simulated time-series of sulfate, nitrate, and ammonium are also in good agreement with observations, with IOA of 0.83, 0.87, and 0.90, respectively. The model considerably overestimates the inorganic aerosol mass concentrations from 16 to 18 January. One of the possible reasons is the decreased emissions, particularly from industries before the Chinese New Year, which are not reflected in the emission inventory used in the study.

Figure 7 presents the contributions of aerosol species to the simulated $PM_{2.5}$ concentration in BTH and Beijing averaged from 9 to 25 January 2014. The modeled $PM_{2.5}$ mass concentration averaged during the simulation period in BTH and Beijing is 111.6 and 97.7 μg m^{-3}, respectively. OA dominate the $PM_{2.5}$ in BTH, with a contribution of around 43.1%. Although the simulated O_3 concentration is low, the secondary aerosols, including SOA, sulfate, nitrate, and ammonium still make up about 40% of the $PM_{2.5}$ mass concentration, with contributions of 7.9%, 11.3%, 12.4%, and 9.6%, respectively. Elemental carbon and the unspecified aerosol species account for 7.5% and 16.2% of the $PM_{2.5}$ mass concentration,

respectively. In Beijing, sulfate, nitrate, and ammonium constitutes 10.6%, 14.0%, and 9.1% of the $PM_{2.5}$ mass concentrations, respectively. OA are also the dominant constituent of the simulated $PM_{2.5}$ in Beijing, with a contribution of about 44.1%. The simulated ratio of the primary to secondary OA in Beijing is 4.6, which is close to the observed ratio of 4.3. The simulated chemical composition in Beijing is generally comparable to the observation in January 2013 by Huang et al. (2014), showing that OA constitutes a major fraction (40.7%) of the total $PM_{2.5}$, followed by sulfate (16.0%), nitrate (12.0%), and ammonium (9.8%). It is worth noting that the simulated sulfate contribution to $PM_{2.5}$ mass concentrations in Beijing is lower than the observation in Huang et al. (2014), and vice versa for the nitrate aerosol. Implementation of the APPCAP since 2013 September has considerably decreased SO_2 emissions in BTH, lowering the sulfate formation. Additionally, the decrease of the sulfate aerosol reduces its competition with ammonia in the atmosphere, facilitating the nitrate formation.

The good agreements of the simulated mass concentrations of air pollutants with observations at ambient monitoring sites in BTH and aerosol species with HR-ToF-AMS measurements in Beijing show that the simulated wind fields and emission inventory used in present study are generally reasonable, providing a reliable base for further evaluations.

3.2 Contributions of the RCC emission to the air quality in BTH

The contribution of the residential coal combustion (RCC) emission to the air quality in BTH is investigated by the sensitivity study without RCC emissions in BTH and its surrounding areas compared to the reference simulation. Figure 8 shows the spatial distribution of the average contribution of the RCC emission in BTH to $PM_{2.5}$ mass concentrations during the simulation period (REF - SEN-BTH). The RCC emission plays an important role in the $PM_{2.5}$ level in the plain area of BTH, with contributions varying from 30 to 70 μg m^{-3}. Over the mountain areas of BTH, the contribution of RCC emissions to the $PM_{2.5}$ mass concentration

316 is generally less than 10 μg m^{-3}.

317 Table 3 presents the average change of air pollutants mass concentrations during the
318 simulation period in BTH and Beijing. The average $PM_{2.5}$ mass concentration is 111.6 μg m^{-3}
319 in BTH in REF case and decreased to be 85.8 μg m^{-3} in SEN-BTH case when the RCC emission
320 in BTH is excluded. The RCC emission contributes about 23.1% of $PM_{2.5}$ mass concentrations
321 in BTH on average. In addition, the RCC emission is an important source of SO_2 and CO,
322 contributing about 35.8% of SO_2 and 22.5% of CO mass concentrations. The RCC emission
323 does not substantially influence the NO_2 level in BTH, with a contribution of 4.2%. When the
324 RCC emission in BTH is not considered, the O_3 concentration slightly increases due to the
325 decrease of NO_2 concentration. The $PM_{2.5}$ mass concentration is decreased by around 30% in
326 Beijing on average when the RCC emission in BTH is excluded, showing that the air quality
327 in Beijing would be remarkably improved if the residential coal in BTH and its surrounding
328 areas could be replaced by other clean energy sources, such as natural gas or electricity.
329 Furthermore, the RCC emission in BTH contributes about 42.6% of SO_2 and 26.5% of CO
330 mass concentrations in Beijing.

331 Figure 9 shows the average chemical composition of $PM_{2.5}$ contributed by the RCC
332 emission in BTH and Beijing during the simulation period. The RCC emission contributes
333 about 25.8 μg m^{-3} $PM_{2.5}$ in BTH on average, of which about 42.8% is from OA. The sulfate
334 aerosol constitutes 17.1% of the $PM_{2.5}$ from the RCC emission, exceeding the contribution
335 from unidentified aerosol species (15.8%), element carbon (11.5%), ammonium (9.5%) and
336 nitrate (3.3%) aerosol. The results indicate that the priority to mitigate effects of the RCC
337 emission on the air quality in BTH is to decrease the emissions of OA and SO_2 from RCC. In
338 Beijing, OA is still the major contributor to $PM_{2.5}$ from the RCC emission, accounting for about
339 48.5%, which is more than that averaged in BTH. The sulfate and ammonium contribution to
340 the $PM_{2.5}$ from the RCC emission is 13.3% and 7.2%, respectively. The chemical composition

of the $PM_{2.5}$ from the RCC emission in Beijing shows more contribution of OA and less contribution of SO_2 from Beijing local RCC emission. It is worth noting that light absorbing aerosols are thought to alter the ambient temperature profile locally (Wang et al., 2013; Zhang et al., 2015; Peng et al., 2016). The sensitivity results indicate that if the RCC emission in BTH and its surrounding areas is excluded, the surface temperature in BTH is decreased by about 0.23℃ on average during the study period, about half of which is contributed by light absorbing aerosols.

3.3 Contributions of local RCC emission to the air quality in Beijing

As the capital of China, the air quality in Beijing often becomes the focus of attention in China or globally. Beijing is situated at the northern tip of the North China Plain (NCP), one of the most polluted areas in China, caused by rapid industrialization and urbanization (Zhang et al., 2013). In addition, Beijing is surrounded from southwest to northeast by the Taihang Mountains and the Yanshan Mountains which block the dispersion of air pollutants when south or east winds are prevalent in NCP (Long et al., 2016). Therefore, in addition to the contribution of local emissions, the air quality in Beijing is also substantially influenced by the transport of air pollutants from outside (Wu et al., 2017).

Since implementation of the APPCAP issued in September 2013, Beijing has carried out aggressive emission control strategies to improve air quality. Great efforts have been made to replace coal used in residential living by natural gas or electricity, which is highly anticipated to clean the air in Beijing. However, frequent occurrence of heavy haze with extremely high levels of $PM_{2.5}$ during the wintertime of 2015 and 2016 has caused controversial issue about the effect of the coal replacement plan in Beijing. Therefore, a further sensitivity study has been performed in this study, in which only the RCC emission in Beijing is excluded (SEN-PEK) to explore the contribution of the local RCC emission in Beijing to the haze formation. Comparisons of the REF case with the SEN-PEK case show that when the RCC emission in

366 Beijing is not considered or the residential coal is replaced by other clean energy sources, the
367 local $PM_{2.5}$ level decreases from 97.7 to 80.1 μg m^{-3} or by 18.0% on average during the
368 simulation period. The average decreases in SO_2 and CO concentrations are 24.2% and 19.9%,
369 respectively. It is worthy to note that the electricity is principally from the coal burning in China,
370 and the main air pollutants emitted from coal-burning power plants are NO_x and SO_2. However,
371 the major pollutants emitted by the residential coal combustion include organic carbon, SO_2
372 and NO_x. Considering the dominant role of OA in the $PM_{2.5}$ in Beijing, the coal replacement in
373 residential living is more effective in power plants. Therefore, the coal replacement plan in
374 Beijing can improve the local air quality considerably, but is not as expected to substantially
375 improve the air quality.

376 It is still debatable on whether local emissions or transport dominates the air quality in
377 Beijing (Guo et al., 2010, 2014; Li et al., 2015; Zhang et al., 2015; Wu et al., 2017). Sensitivity
378 studies show that when only the RCC emission in Beijing is excluded in simulations, the $PM_{2.5}$
379 level is decreased by 18%, much less than about 30% decrease caused by the exclusion of the
380 RCC emission in BTH and its surrounding areas, showing the important contribution of trans-
381 boundary transport to the air quality in Beijing. Analyses are further made to examine the
382 contribution of the RCC emission in Beijing to the $PM_{2.5}$ mass concentrations under different
383 pollution levels. The simulated hourly near-surface $PM_{2.5}$ mass concentrations in REF case
384 during the whole episode in Beijing are first subdivided into 6 bins according to the air quality
385 standard in China for $PM_{2.5}$ (Feng et al., 2016), i.e., 0~35 (excellent), 35~75 (good), 75~115
386 (lightly polluted), 115~150 (moderately polluted), 150~250 (heavily polluted), and greater than
387 250 (severely polluted) μg m^{-3}. $PM_{2.5}$ mass concentrations in REF case and SEN-PEK case as
388 the bin $PM_{2.5}$ concentrations in REF case following the grid cells are assembled respectively,
389 and an average of $PM_{2.5}$ mass concentrations in each bin is calculated. Figure 10 presents the
390 contribution of the RCC emission in Beijing to the local $PM_{2.5}$ mass concentrations. Apparently,

391 the mitigation effect is the best under good and lightly polluted conditions in terms of $PM_{2.5}$
392 level, and the $PM_{2.5}$ mass concentration decreases by around 25% when the RCC emission in
393 Beijing is not considered, indicating that the local RCC emission does not constitute the main
394 $PM_{2.5}$ pollution source in Beijing. However, with the deterioration of haze pollution from
395 moderately to severely polluted conditions, the $PM_{2.5}$ contribution from the local RCC
396 emission in Beijing decreases from 20% to 15%, showing the regional transport of $PM_{2.5}$.
397
398 **4 Summary and Conclusions**
399 In the present study, a persistent air pollution episode in BTH from 9 to 25 January 2014
400 is simulated using the WRF-Chem model to assess contributions of the RCC emission to the
401 air quality in BTH. In general, the WRF-Chem model performs well in simulating the temporal
402 variations and spatial distributions of air pollutants when compared with observations over
403 monitoring sites in BTH. The simulated diurnal variations of aerosol species are also in good
404 agreements with the HR-ToF-AMS measurements in Beijing.
405 Sensitivity studies show that, on average, the RCC emission contributes about 23.1% of
406 $PM_{2.5}$ mass concentrations in BTH during the simulation period and is also an important SO_2
407 and CO source, accounting for about 35.8% of SO_2 and 22.5% of CO mass concentrations. OA
408 is the major contributor to $PM_{2.5}$ from the RCC emission, with a contribution of 42.8%,
409 followed by sulfate (17.1%), unspecified species (15.8%), element carbon (11.5%), ammonium
410 (9.5%) and nitrate (3.3%) aerosol. Exclusion of the RCC emission in BTH decreases the $PM_{2.5}$
411 concentration by around 30% in Beijing, indicating that the air quality in Beijing will be
412 remarkably improved if the residential coal in BTH and its surrounding areas can be replaced
413 by other clean energy sources.
414 When only the RCC emission in Beijing is excluded in simulations, Beijing's $PM_{2.5}$ level
415 decreases by 18.0% on average during the simulation period. Hence, the coal replacement plan

in Beijing is beneficial to the local air quality, but is not as anticipated to substantially improve the air quality. The mitigation effect of the coal replacement plan on $PM_{2.5}$ in Beijing is the best under good and lightly polluted conditions, decreasing the $PM_{2.5}$ mass concentration by around 25%. However, under heavy or severe haze pollution, the local RCC emission contributes about 15% of $PM_{2.5}$ in Beijing, showing the regional transport of $PM_{2.5}$.

This study mainly aims to quantitatively evaluate the contributions of the RCC emission to the air quality in BTH. Our results indicate that if the residential coal replacement is only implemented in Beijing, Beijing's air quality will be improved considerably, but not substantially, considering the impact of trans-boundary transport. Implementation of the residential coal replacement in BTH and its surrounding areas can remarkably improve Beijing's air quality. Although the WRF-Chem model reasonably captures the temporal and spatial variations of air pollutants in BTH and diurnal variations of aerosol species in Beijing, the model biases still exit. Future studies need to be conducted to improve the WRF-Chem model simulations, considering the rapid changes in anthropogenic emissions since the implementation of APPCAP. Further sensitivity simulations of various emission mitigation measures also need to be performed to provide efficient emission control strategies to improve the air quality in BTH.

5 Data availability

The real-time O_3 and $PM_{2.5}$ mass concentrations are accessible to the public on website http://106.37.208.233:20035/ (China MEP, 2013a). One can also access the historic profiles of the observed ambient air pollutants by visiting http://www.aqistudy.cn/ (China MEP, 2013b).

Acknowledgements. This work is financially supported by the National Key R&D Plan (Quantitative Relationship and Regulation Principle between Regional Oxidation Capacity of

441 Atmospheric and Air Quality (2017YFC0210000)). Guohui Li is supported by “Hundred
442 Talents Program” of the Chinese Academy of Sciences and the National Natural Science
443 Foundation of China (No. 41661144020).

444
445

References

An, X., Zhu, T., Wang, Z., Li, C., and Wang, Y., 2007. A modeling analysis of a heavy air pollution episode occurred in Beijing. *Atmospheric Chemistry and Physics,* 7(12), 3103-3114, doi: 10.5194/acp-7-3103-2007.

Archernicholls, S., Carter, E. M., Kumar, R., Xiao, Q., Yang, L., Frostad, J., Forouzanfar, M. H., Cohen, A., Brauer, M., Baumgartner, J., and Wiedinmyer, C., 2016. The regional impacts of cooking and heating emissions on ambient air quality and disease burden in China. *Environmental Science and Technology,* 50(17), 9416-8423, doi: 10.1021/acs.est.6b02533.

Bei, N., Li, G., Zavala, M., Barrera, H., Torres, R., Grutter, M., Gutierrez, W., Garcia, M., Ruiz-Suarez, L. G., Ortinez, A., Guitierrez, Y., Alvarado, C., Flores, I., and Molina, L. T., 2013. Meteorological overview and plume transport patterns during Cal-Mex 2010. *Atmospheric Environment,* 70, 477-489, doi: 10.1016/j.atmosenv.2012.01.065.

Bei, N., Li, G., and Molina, L. T., 2012. Uncertainties in SOA simulations due to meteorological uncertainties in Mexico City during MILAGRO-2006 field campaign. *Atmospheric Chemistry and Physics,* 12, 11295-11308, doi: 10.5194/acp-12-11295-2012.

Bei, N., Wu, J., Elser, M., Feng, T., Cao, J., El-Haddad, I., Li, X., Huang, R., Li, Z., Long, X., Xing, L., Zhao, S., Tie, X., Prévôt, A. S. H., and Li, G., 2017. Impacts of meteorological uncertainties on the haze formation in Beijing-Tianjin-Hebei (BTH) during wintertime: a case study. *Atmospheric Chemistry and Physics,* 17, 14579-14591, doi: 10.5194/acp-17-14579-2017.

Boylan, J. W., and Russell., A. G., 2006. PM and light extinction model performance metrics, goals, and criteria for three-dimensional air quality models. *Atmospheric Environment,* 40 (26), 4946-4959, doi: 10.1016/j.atmonsenv.2005.09.087.

BP: Statistical Review of World Energy 2016.

Canonaco, F., Crippa, M., Slowik, J. G., Baltensperger, U., and Prévôt, A. S. H., 2013. Sofi, an IGOR-based interface for the efficient use of the generalized multilinear engine (ME-2) for the source apportionment: ME-2 application to aerosol mass spectrometer data. *Atmospheric Measurement Techniques,* 6(12), 3649-3661, doi: 10.5194/amt-6-3649-2013.

Chen, F. and Dudhia, J., 2001. Coupling an advanced land surface-hydrology model with the Penn State-NCAR MM5 modeling system. Part I: Model implementation and sensitivity. *Monthly Weather Review,* 129(4), 569-585, doi: 10.1175/1520-0493(2001)129<0569:caalsh>2.0.co;2.

Chen, Y., Schleicher, N., Cen, K., Liu, X., Yu, Y., Zibat, V., Dietze, V., Fricker, M., Kaminski, U., Chen, Y., Chai, F., Norra, S., 2016. Evaluation of impact factors on $PM_{2.5}$ based on long-term chemical components analyses in the megacity Beijing, China. *Chemosphere,* 155, 234-42, doi: 10.1016/j.chemosphere.2016.04.052.

Cheng, M., Zhi, G., Tang, W., Liu, S., Dang, H., Guo, Z., Du, J., Du, X., Zhang, W., Zhang, Y., and Meng, F., 2016. Air pollutant emission from the underestimated households' coal consumption source in China. *Science of the Total Environment,* 580, 641-650, doi:

10.1016/j.scitotenv.2016.12.143.

Chinese State Council. Atmospheric Pollution Prevention and Control Action Plan, 2013 (in Chinese).

Chou, M. D. and Suarez, M. J., 1999. A solar radiation parameterization for atmospheric studies, NASA/TM-10460. *Nasa Technical memo,* 15.

Chou, M. D. and Suarez, M. J., 2001. A thermal infrared radiation parameterization for atmospheric studies, NASA/TM-104606. *Max J,* 19.

Dunker, A. M., Morris, R. E., Pollack, A. K., Schleyer, C. H., and Yarwood, G., 1996. Photochemical modeling of the impact of fuels and vehicles on urban ozone using auto oil program data, *Environmental Science and Technology,* 30, 787-801.

Elser, M., Huang, R., Wolf, R., Slowik, J. G., Wang, Q., Canonaco, F., Li, G., Bozzetti, C., Daellenbach, K. R., Huang, Y., Zhang, R., Li, Z., Cao, J., Baltensperger, U., El-Haddad, I., and Prévôt, A. S. H., 2016. New insights into $PM_{2.5}$ chemical composition and sources in two major cities in China during extreme haze events using aerosol mass spectrometry. *Atmospheric Chemistry and Physics,* 16, 3207-3225, doi: 10.5194/acp-16-3207-2016.

Emery, C., Liu, Z., Russell, A. G., Odman, M. T., Yarwood, G., Kumar, N., 2016. Recommendations on statistics and benchmarks to assess photochemical model performance. *Journal of the Air and Waste Management Association,* 67(5), 582-598, doi: 10.1080/10962247.2016.1265027.

EPA, U.S., 2005. Guidance on the Use of Models and Other Analyses in Attainment Demonstrations for the 8-hour Ozone. NAAQS, EPA454/R-05-002.

Fast, J. D., Jr, W. I. G., Easter, R. C., Zaveri, R. A., Barnard, J. C., Chapman, E. G., Grell, G. A., and Peckham, S. E., 2006. Evolution of ozone, particulates, and aerosol direct radiative forcing in the vicinity of Houston using a fully coupled meteorology-chemistry-aerosol model. *Journal of Geophysical Research-Atmospheres,* 111(D21), doi: 10.1029/2005JD006721.

Feng, T., Li, G., Cao, J., Bei, N., Shen, Z., Zhou, W., Liu, S., Zhang, T., Wang, Y., Huang, R., Tie, X., and Molina, L. T., 2016. Simulations of organic aerosol concentrations during springtime in the Guanzhong Basin, China. *Atmospheric Chemistry and Physics,* 16, 10045-10061, doi: 10.5194/acp-16-10045-2016.

Gao, M., Carmichael, G. R., Wang, Y., Saide, P. E., Yu, M., Xin, J., Liu, Z., and Wang, Z., 2016. Modeling study of the 2010 regional haze event in the North China Plain, *Atmospheric Chemistry and Physics,* 16(3), 1673-1691, doi: 10.5194/acp-16-1673-2016.

Ge, S., Xu, X., Chow, J.C., Watson, J., Sheng, Q., Liu, W., Bai, Z., Zhu, T., and Zhang, J., 2004. Emissions of air pollutants from household Stoves: honeycomb coal versus coal cake. *Environmental Science and Technology,* 38(17), 4612-4618, doi: 10.1021/es049942k.

Grell, G. A., Peckham, S. E., Schmitz, R., McKeen, S. A., Frost, G., Skamarock, W. C., and Eder, B., 2005. Fully coupled "online" chemistry within the WRF model. *Atmospheric Environment*, 39, 6957-6975, doi: 10.1016/j.atmosenv.2005.04.027.

527 Guenther, A., Karl, T., Harley, P., Wiedinmyer, C., Palmer, P. I., and Geron, C., 2006.
528 Estimates of global terrestrial isoprene emissions using MEGAN (Model of Emissions of
529 Gases and Aerosols from Nature). *Atmospheric Chemistry and Physics,* 6, 3181-3210,
530 doi: 10.5194/acp-6-3181-2006.

531 Guo, S., Hu, M., Wang, Z., Slanina, J., and Zhao, Y., 2010. Size-resolved aerosol water-
532 soluble ionic compositions in the summer of Beijing: implication of regional secondary
533 formation. *Atmospheric Chemistry and Physics,* 10, 947-959, doi:10.5194/acp-10-947-
534 2010.

535 Guo, S., Hu, M., Zamora, M. L., Peng, J., Shang, D., Zheng, J., Du, Z. F., Wu, Z., Shao, M.,
536 Zeng, L. M., Molina, M. J., and Zhang, R., 2014. Elucidating severe urban haze
537 formation in China. *Proceedings of the National Academy of Sciences of the United*
538 *States of America,* 111(49), 17373-17378, doi: 10.1073/pnas.1419604111.

539 Hong, S. Y. and Lim, J. O. J., 2006. The WRF Single-Moment 6-Class Microphysics Scheme
540 (WSM6). *Asia-Pacific Journal of Atmospheric Sciences,* 42, 129-151.

541 Horowitz, L. W., Walters, S., Mauzerall, D. L., Emmons, L. K., Rasch, P. J., Granier, C., Tie,
542 X., Lamarque, J. F., Schultz, M. G., Tyndall, G. S., Orlando, J. J., and Brasseur, G. P.,
543 2003. A global simulation of tropospheric ozone and related tracers: Description and
544 evaluation of MOZART, version 2. *Journal of Geophysical Research,* 108, 4784, doi:
545 10.1029/2002jd002853.

546 Huang, R., Zhang, Y., Bozzetti, C., Ho, K. F., Cao, J., Han, Y., Daellenbach, K. R., Slowik, J.
547 G., Platt, S. M., Canonaco, F., Zotter, P., Wolf, R., Pieber, S. M., Bruns, E. A., Crippa,
548 M., Ciarelli, G., Piazzalunga, A., Schwikowski, M., Abbaszade, G., Schnelle-Kreis, J.,
549 Zimmermann, R., An, Z., Szidat, S., Baltensperger, U., El Haddad, I., and Prevot, A. S.
550 H., 2014. High secondary aerosol contribution to particulate pollution during haze events
551 in China. *Nature,* 514(7521), 218-222, doi: 10.1038/nature13774.

552 Janjić, Z. I., 2002. Nonsingular Implementation of the Mellor-Yamada Level 2.5 Scheme in
553 the NCEP Meso Model. *Ncep Office Note,* 436.

554 Lei, Y., Zhang, Q., He, K., and Streets, D. G., 2011. Primary anthropogenic aerosol emission
555 trends for China, 1990-2005. *Atmospheric Chemistry and Physics,* 11(3), 931-954, doi:
556 10.5194/ acp-11-931-2011.

557 Li, G., Bei, N., Tie, X., and Molina, L. T., 2011a. Aerosol effects on the photochemistry in
558 Mexico City during MCMA-2006/MILAGRO campaign. *Atmospheric Chemistry and*
559 *Physics,* 11, 5169-5182, doi: 10.5194/acp-11-5169-2011.

560 Li, G., Lei, W., Zavala, M., Volkamer, R., Dusanter, S., Stevens, P., and Molina, L. T., 2010.
561 Impacts of HONO sources on the photochemistry in Mexico City during the MCMA-
562 2006/MILAGO Campaign. *Atmospheric Chemistry and Physics,* 10, 6551-6567, doi:
563 10.5194/acp-10-6551-2010.

564 Li, G., Zavala, M., Lei, W., Tsimpidi, A. P., Karydis, V. A., Pandis, S. N., Canagaratna, M. R.,
565 and Molina, L. T., 2011b. Simulations of organic aerosol concentrations in Mexico City
566 using the WRF- Chem model during the MCMA-2006/MILAGRO campaign.
567 *Atmospheric Chemistry and Physics,* 11, 3789-3809, doi: 10.5194/acp-11-3789-2011.

568 Li, G., Zhang, R., Fan, J., and Tie, X., 2005. Impacts of black carbon aerosol on photolysis

and ozone. *Journal of Geophysical Research Atmospheres,* 110, D23206, doi: 10.1029/2005JD005898.

Li, J., Huang, X., Yang, H., Chuai, X., Li, Y., Qu, J., and Zhang, Z., 2016. Situation and determinants of household carbon emissions in Northwest China. *Habitat International,* 51, 178-187, doi: 10.1016/j.habitatint.2015.10.024.

Li, M., Zhang, Q., Kurokawa, J. I., Woo, J. H., He, K., Lu, Z., Ohara, T., Song, Y., Streets, D. G., Carmichael, G. R., Cheng, Y., Hong, C., Huo, H., Jiang, X., Kang, S., Liu, F., Su, H., and Zheng, B., 2017. MIX: a mosaic Asian anthropogenic emission inventory under the international collaboration framework of the MICS-Asia and HTAP. *Atmospheric Chemistry and Physics,* 17, 935-963, doi: 10.5194/acp-17-935-2017.

Li, X., Zhang, Q., Zhang, Y., Zheng, B., Wang, K., and Chen, Y. 2015. Source contributions of urban $PM_{2.5}$ in the Beijing-Tianjin-Hebei region: Changes between 2006 and 2013 and relative impacts of emissions and meteorology. *Atmospheric Environment,* 123, 229-239, doi: 10.1016/j.atmosenv.2015.10.048.

Liu, F., Zhang, Q., Tong, D., Zheng, B., Li, M., Huo, H., and He, K., 2015. High-resolution inventory of technologies, activities, and emissions of coal-fired power plants in China from 1990 to 2010. *Atmospheric Chemistry and Physics,* 15(23), 13299-13317, doi:10.5194/acp-15-13299-2015.

Liu, J., Mauzerall, D. L., Chen, Q., Zhang, Q., Song, Y., Peng, W., Klimont, Z., Qiu, X., Zhang, S., Hu, M., Lin, W., Smith, K. R., Zhu, T., 2016. Air pollutant emissions from Chinese households: a major and underappreciated ambient pollution source. *Proceedings of the National Academy of Sciences of the United States of America,* 113(28), 7756-7761, doi: 10.1073/pnas.1604537113.

Long, X., Tie, X., Cao, J., Huang, R., Feng, T., Li, N., Zhao, S., Tian, J., Li, G., and Zhang, Q., 2016. Impact of crop field burning and mountains on heavy haze in the North China Plain: a case study. *Atmospheric Chemistry and Physics,* 16, 9675-9691, doi: 10.5194/acp-16-9675-2016.

Lv, B., Zhang, B., and Bai, Y., 2016. A systematic analysis of $PM_{2.5}$ in Beijing and its sources from 2000 to 2012. *Atmospheric Environment,* 124, 98-108, doi: 10.1016/j.atmosenv.2015.09.031.

Ma, Q., Cai, S., Wang, S., Zhao, B., Martin, R. V., Brauer, M., Cohen, A., Jiang, J., Zhou, W., Hao, J., Frostad, J., Forouzanfar, M. H., and Burnett, R. T., 2017. Impacts of coal burning on ambient $PM_{2.5}$ pollution in China. *Atmospheric Chemistry and Physics,* 17, 4477-4491, doi: 10.5194/acp-17-4477-2017.

Ministry of Environmental Protection of China (MEP): 2013 Report on the State of Environment in China, 2014 (in Chinese).

Ministry of Environmental Protection of China (MEP): 2014 Report on the State of Environment in China, 2015 (in Chinese).

Nenes, A., Pandis, S. N., and Pilinis, C., 1998. ISORROPIA: A new thermodynamic equilibrium model for multiphase multi-component inorganic aerosols. *Aquatic Geochemistry,* 4, 123-152, doi: 10.1023/a:1009604003981.

Peng, J., Hu, M., Guo, S., Du, Z., Shang, D., Zheng, J., Zheng, J., Zeng, L., Shao, M., Wu, Y., Collins, D., and Zhang, R., 2017. Ageing and hygroscopicity variation of black carbon particles in Beijing measured by a quasi-atmospheric aerosol evolution study (QUALITY) chamber, *Atmospheric Chemistry and Physics,* 17, 10333-10348, doi: 10.5194/acp-17-10333-2017.

Qiao, X., Ying, Q., Li, X., Zhang, H., Hu, J., Tang, Y., and Chen, X., 2017. Source apportionment of $PM_{2.5}$ for 25 Chinese provincial capitals and municipalities using a source-oriented Community Multiscale Air Quality model. *Science of the Total Environment,* 612, 462-471, doi: 10.1016/j.scitotenv.2017.08.272.

Quan, J., Tie, X., Zhang, Q., Liu, Q., Li, X., Gao, Y., and Zhao, D., 2014. Characteristics of heavy aerosol pollution during the 2012-2013 winter in Beijing, China. *Atmospheric Environment,* 88(5), 83-89, doi: 10.1016/j.atmosenv.2014.01.058.

Seinfeld, J. H. and Pandis, S. N., 2006. Atmospheric Chemistry and Physics: From Air Pollution to Climate Change, 2nd Edition. *Wiley*.

Sheehan, P., Cheng, E., English, A., and Sun, F., 2014. China's response to the air pollution shock. *Nature Climate Change,* 4(5):306-309, doi: 10.1038/nclimate2197.

Shen, G., Yang, Y., Wang, W., Tao, S., Zhu, C., Min, Y., Xue, M., Ding, J., Wang, B., Wang, R., Shen, H., Li, W., Wang, X., and Russell, A. G., 2010. Emission factors of particulate matter and elemental carbon for crop residues and coals burned in typical household stoves in China. *Environmental Science and Technology,* 44(18), 7157-7162, doi: 10.1021/es101313y.

Tie, X., Madronich, S., Walters, S., Zhang, R., Rasch, P., and Collins, W., 2003. Effect of clouds on photolysis and oxidants in the troposphere. *Journal of Geophysical Research,* 108, 4642, doi: 10.1029/2003jd003659.

Wang, C., 2013. Impact of anthropogenic absorbing aerosols on clouds and precipitation: a review of recent progresses. *Atmospheric Research,*122(3), 237-249, doi: 10.1016/j.atmosres.2012.11.005.

Wang, G., Zhang, R., Gomez, M. E., Yang, L., Zamora, M. L., Hu, M., Lin, Y., Peng, J., Guo, S., Meng, J., Li, J., Cheng, C., Hu, T., Ren, Y., Wang, Y., Gao, J., Cao, J., An, Z., Zhou, W., Li, G., Wang, J., Tian, P., Marrero-Ortiz, W., Secrest, J., Du, Z., Zheng, J., Shang, D., Zeng, L., Shao, M., Wang, W., Huang, Y., Wang, Y., Zhu, Y., Li, Y., Hu, J., Pan, B., Cai, L., Cheng, Y., Ji, Y., Zhang, F., Rosenfeld, D., Liss, P. S., Duce, R. A., Kolb, C. E., and Molina, M. J., 2016. Persistent sulfate formation from London fog to Chinese haze. *Proceedings of the National Academy of Sciences of the United States of America,* 113(48), 13630-13635, doi: 10.1073/pnas.1616540113.

Wang, L., Wei, Z., Yang, J., Zhang, Y., Zhang, F., Su, J., Meng, C., and Zhang, Q., 2014. The 2013 severe haze over southern Hebei, China: model evaluation, source apportionment, and policy implications, *Atmospheric Chemistry and Physics,* 14, 3151-3173, doi: 10.5194/acp-14-3151-2014.

Wang, L., Xu, J., Yang, J., Zhao, X., Wei, W., Cheng, D., Pan, X., and Su, J., 2012. Understanding haze pollution over the southern Hebei area of China using the CMAQ model. *Atmospheric Environment,* 56(5), 69-79, doi: 10.1016/j.atmosenv.2012.04.013.

Wang, X., Carmichael, G., Chen, D., Tang, Y., and Wang, T., 2005. Impacts of different emission sources on air quality during March 2001 in the Pearl River Delta (PRD) region. *Atmospheric Environment,* 39, 5227-5241, doi: 10.1016/j.atmosenv.2005.04.035.

Wesely, M. L., 1989. Parameterization of surface resistances to gaseous dry deposition in regional-scale numerical models. *Atmospheric Environment,* 23, 1293-1304, doi: 10.1016/0004-6981(89)90153-4.

WHO, (World Trade Organization), 2005. Air Quality Guidelines for Particulate Matter, Ozone, Nitrogen Dioxide and Sulfur Dioxide.

Williams, L. R., Gonzalez, L. A., Peck, J., Trimborn, D., McInnis, J., Farrar, M. R., Moore, K. D., Jayne, J. T., Robinson, W. 80 A., Lewis, D. K., Onasch, T. B., Canagaratna, M. R., Trimborn, A., Timko, M. T., Magoon, G., Deng, R., Tang, D., de la Rosa Blanco, E., Prévôt, A. S. H., Smith, K. A., and Worsnop, D. R., 2013. Characterization of an aerodynamic lens for transmitting particles greater than 1 micrometer in diameter into the Aerodyne 85 aerosol mass spectrometer. *Atmospheric Measurement Techniques,* 6, 3271-3280, https://doi.org/10.5194/amt-6-3271-2013.

Wornat, M. J., Ledesma, E. B., Sandrowitz, A. K., Roth, M. J., Dawsey, S. M., Qiao, Y. L., and Chen, W., 2001. Polycyclic aromatic hydrocarbons identified in soot extracts from domestic coal-burning stoves of Henan province, China. *Environmental Science and Technology,* 35(10), 1943-1952, doi: 10.1021/es001664b.

Wu, J., Li, G., Cao, J., Bei, N., Wang, Y., Feng, T., Huang, R., Liu, S., Zhang, Q., and Tie, X., 2017. Contributions of trans-boundary transport to summertime air quality in Beijing, China. *Atmospheric Chemistry and Physics,* 17, 2035-2051, doi:10.5194/acp-17-2035-2017.

Xue, Y., Zhou, Z., Nie, T., Wang, K., Nie, L., Pan, T., Wu, X., Tian, H., Zhong, L., Li, J., Liu, H., Liu, S., and Shao, P., 2016. Trends of multiple air pollutants emissions from residential coal combustion in Beijing and its implication on improving air quality for control measures. *Atmospheric Environment,* 142, 303-312, doi: 10.1016/j.atmosenv.2016.08.004.

Yang, H., Chen, J., Wen, J., Tian, H., and Liu, X., 2016. Composition and sources of $PM_{2.5}$, around the heating periods of 2013 and 2014 in Beijing: implications for efficient mitigation measures. *Atmospheric Environment,* 124, 378-386, doi: 10.1016/j.atmosenv.2015.05.015.

Zhang, H., and Ying, Q., 2011. Contributions of local and regional sources of NO_x to ozone concentrations in Southeast Texas. *Atmospheric Environment*, 45(17), 2877-2887.

Zhang, L., Liu, L., Zhao, Y., Gong, S., Zhang, X., Henze, D. K., Capps, S. L., Fu, T., Zhang, Q. and Wang, Y., 2015. Source attribution of particulate matter pollution over North China with the adjoint method. *Environmental Research Letters,* 10(8), 084011, doi: 10.1088/1748-9326/10/8/084011.

Zhang, L., Wang, T., Lv, M., and Zhang, Q., 2015. On the severe haze in Beijing during January 2013: unraveling the effects of meteorological anomalies with WRF-Chem. *Atmospheric Environment,* 104, 11-21, doi: 10.1016/j.atmosenv.2015.01.001.

Zhang, Q., He, K., and Huo, H., 2012. Policy: cleaning china's air. *Nature,* 484(7393), 161-

162, doi: 10.1038/484161a.

Zhang, Q., Streets, D. G., Carmichael, G. R., He, K., Huo, H., Kannari, A., Klimont, Z., Park, I. S., Reddy, S., Fu, J., Chen, D., Duan, L., Lei, Y., Wang, L., and Yao, Z., 2009. Asian emissions in 2006 for the NASA INTEX-B mission. *Atmospheric Chemistry and Physics,* 9, 5131-5153, doi: 10.5194/acp-9-5131-2009.

Zhang, R., Jing, J., Tao, J., Hsu, S. C., Wang, G., Cao, J., Lee, C. S. L., Zhu, L., Chen, Z., Zhao, Y., and Shen, Z., 2013. Chemical characterization and source apportionment of $PM_{2.5}$ in Beijing: seasonal perspective. *Atmospheric Chemistry and Physics,* 13, 7053-7074, doi:10.5194/acp-13-7053-2013.

Zhang, R., Wang, L., Khalizova, A. F., Zhao, J., Zheng, J., Mc-Grawb, R. L., and Molina, L. T., 2009. Formation of nanoparticles of blue haze enhanced by anthropogenic pollution. *Proceedings of the National Academy of Sciences of the United States of America,* 106, 17650-17654.

Zhang, X., Kim, H., Parworth, C. L., Young, D. E., Zhang, Q., Metcalf, A. R., and Cappa, C. D., 2016. Optical properties of wintertime aerosols from residential wood burning in Fresno, CA: results from DISCOVER-AQ 2013. *Environmental Science and Technology,* 50(4), 1681-1690, doi: 10.1021/acs.est.5b04134.

Zhang, X., Wang, Y., Niu, T., Zhang, X., Gong, S., Zhang, Y., and Sun, J., 2012. Atmospheric aerosol compositions in China: spatial/temporal variability, chemical signature, regional haze distribution and comparisons with global aerosols. *Atmospheric Chemistry and Physics,* 11(14), 26571-26615, doi: 10.5194/acpd-11-26571-2011.

Zhi, G., Chen, Y., Feng, Y., Xiong, S., Li, J., Zhang, G., Sheng, G., and Fu, J., 2008. Emission characteristics of carbonaceous particles from various residential coal-stoves in China. *Environmental Science and Technology,* 42(9), 3310-3315, doi: 10.1021/es702247q.

Zíková, N., Wang, Y., Yang, F., Li, X., Tian, M., and Hopke, P. K., 2016. On the source contribution to Beijing $PM_{2.5}$ concentrations. *Atmospheric Environment,* 134, 84-95, doi: 10.1016/j.atmosenv.2016.03.047.

723 Table 1 WRF-Chem model configurations.
724

Region	**Beijing-Tianjin-Hebei (BTH)**
Simulation period	January 9 to 26, 2014
Domain size	150 × 150
Domain center	39°N, 117°E
Horizontal resolution	6km × 6km
Vertical resolution	35 vertical levels with a stretched vertical grid with spacing ranging from 30 m near the surface, to 500 m at 2.5 km and 1 km above 14 km
Microphysics scheme	WSM 6-class graupel scheme (Hong and Lim, 2006)
Boundary layer scheme	MYJ TKE scheme (Janjić, 2002)
Surface layer scheme	MYJ surface scheme (Janjić, 2002)
Land-surface scheme	Unified Noah land-surface model (Chen and Dudhia, 2001)
Longwave radiation scheme	Goddard longwave scheme (Chou and Suarez, 2001)
Shortwave radiation scheme	Goddard shortwave scheme (Chou and Suarez, 1999)
Meteorological boundary and initial conditions	NCEP 1°×1° reanalysis data
Chemical initial and boundary conditions	MOZART 6-hour output (Horowitz et al., 2003)
Anthropogenic emission inventory	Developed by Zhang et al. (2009) and Li et al. (2017)
Biogenic emission inventory	MEGAN model developed by Guenther et al. (2006)

725
726

Table 2 Validation of WRF-Chem model performance on simulations of air pollutants.

Species	FB[a]		FE[b]		NMB[c]		NME[d]		r[e]	
	This study	Ref. criteria	This study	Ref. criteria	This study	Ref. criteria	This study	Ref. criteria	This study	Ref. criteria
$PM_{2.5}$	-0.7%	< ±60%[1]	21.5%	<±75%[1]	-1.7%	<±30%[2]	18.5%	<±50%[2]	0.89	>0.40[2]
O_3	-28.0%		40.5%		-11.3%	<±15%[3]	24.7%	<±35%[3]	0.91	>0.50[3]
OA	21.7%	< ±60%[1]	51.9%	<±75%[1]	8.6%	<±50%[2]	44.5%	<±65%[2]	0.74	
CCOA	39.0%	< ±60%[1]	64.7%	<±75%[1]	21.5%	<±50%[2]	59.6%	<±65%[2]	0.69	
Sulfate	46.5%	< ±60%[1]	64.7%	<±75%[1]	37.6%	<±30%[2]	67.8%	<±50%[2]	0.75	>0.40[2]
Nitrate	6.0%	< ±60%[1]	56.2%	<±75%[1]	-1.3%	<±65%[2]	46.5%	<±115%[2]	0.78	
Ammonium	11.5%	< ±60%[1]	46.3%	<±75%[1]	-2.7%	<±30%[2]	37.4%	<±50%[2]	0.83	>0.40[2]

[a] Fractional bias (FB): $FB = \frac{2}{N}\sum\frac{(P_j - O_j)}{(P_j + O_j)} \times 100$

[b] Fractional error (FE): $FE = \frac{2}{N}\sum\frac{|P_j - O_j|}{(P_j + O_j)} \times 100$

[c] Normalized mean bias (NMB): $NMB = \frac{\sum(P_j - O_j)}{\sum O_j} \times 100$

[d] Normalized mean error (NME): $NME = \frac{\sum|P_j - O_j|}{\sum O_j} \times 100$

[e] Correlation coefficient (r): $r = \frac{\sum[(P_j - \bar{P}) \times (O_j - \bar{O})]}{\sqrt{\sum(P_j - \bar{P})^2 \times \sum(O_j - \bar{O})^2}}$

Where subscript j represents the pairing of N, observations O, and predictions P, by site and time. r = 1 is perfect correlation, r = 0 is totally uncorrelated.

[1] Boylan and Russell (2006)
[2] Emery et al. (2017)
[3] US EPA (2005)

Table 3 Average mass concentrations of air pollutants in REF case and SEN-BTH case from 9 to 25 January 2014 in BTH and Beijing. (Unit: μg m^{-3} for $PM_{2.5}$, O_3, NO_2, SO_2 and mg m^{-3} for CO)

Air pollutants	BTH				Beijing			
	REF	SEN-BTH	Mass change	Percentage change	REF	SEN-BTH	Mass change	Percentage change
$PM_{2.5}$	111.6	85.8	25.8	23.1%	97.7	68.9	28.8	29.5%
O_3	39.1	39.4	-0.3	-0.8%	39.3	39.8	-0.5	-1.3%
NO_2	45.7	43.7	2.0	4.3%	51.5	49.4	2.1	4.1%
SO_2	45.0	28.9	16.1	35.8%	42.2	24.2	18.0	42.6%
CO	1.7	1.3	0.4	22.5%	1.5	1.1	0.4	26.5%

Figure Captions

Figure 1 (a) Map showing the location of Beijing-Tianjin-Hebei and (b) WRF-Chem model simulation domain with topography. In (b), the filled red circles represent centers of cities with ambient monitoring site and the size of the circle denotes the number of ambient monitoring sites of cities. The filled black rectangle denotes the deployment location of the HR-ToF-AMS in Beijing. The three filled black circles represent the location of the meteorological observation stations in Beijing, Tianjin, and Shijiazhuang, respectively.

Figure 2 Comparisons of observed (black dots) and simulated (solid red lines) diurnal profiles of near-surface temperature (T), relative humidity (RH), wind speed (WS), and wind direction (WD) at meteorological sites in (a) Beijing, (b) Tianjin, and (c) Shijiazhuang from 9 to 25 January 2014.

Figure 3 Pattern comparisons of simulated (color counters) vs. observed (colored circles) near-surface mass concentrations of (a) $PM_{2.5}$, (b) O_3, (c) NO_2, and (d) SO_2 averaged from 9 to 25 January 2014. The black arrows indicate simulated surface winds.

Figure 4 Comparisons of observed (black dots) and simulated (solid red lines) diurnal profiles of near-surface hourly mass concentrations of (a) $PM_{2.5}$, (b) O_3, (c) NO_2, (d) SO_2, and (d) CO averaged at monitoring sites in BTH from 9 to 25 January 2014.

Figure 5 Scatter plots of the (a) observed and (b) simulated $PM_{2.5}$ with CO mass concentrations averaged over all ambient monitoring sites in BTH from 9 to 25 January 2014.

Figure 6 Comparisons of measured (black dots) and simulated (solid red lines) diurnal profiles of (a) organic aerosol (OA), (b) coal combustion organic aerosol (CCOA), (c) sulfate, (d) nitrate, and (e) ammonium in Beijing from 9 to 25 January 2014.

Figure 7 Chemical composition of $PM_{2.5}$ averaged from 9 to 25 January 2014 in (a) BTH and (b) Beijing.

Figure 8 Spatial distribution of the average contribution of the RCC emission in BTH to $PM_{2.5}$ mass concentrations from 9 to 25 January 2014.

Figure 9 Chemical composition of $PM_{2.5}$ from the RCC emission in BTH averaged from 9 to 25 January 2014 in (a) BTH and (b) Beijing.

Figure 10 Average contributions of the RCC emission in Beijing to the local $PM_{2.5}$ mass concentrations under different haze pollution levels from 9 to 25 January 2014. *The green, yellow, orange, red, purple, and dark red represents excellent, good, slightly polluted, moderately polluted, heavily polluted, and severely polluted levels of air quality, respectively.*

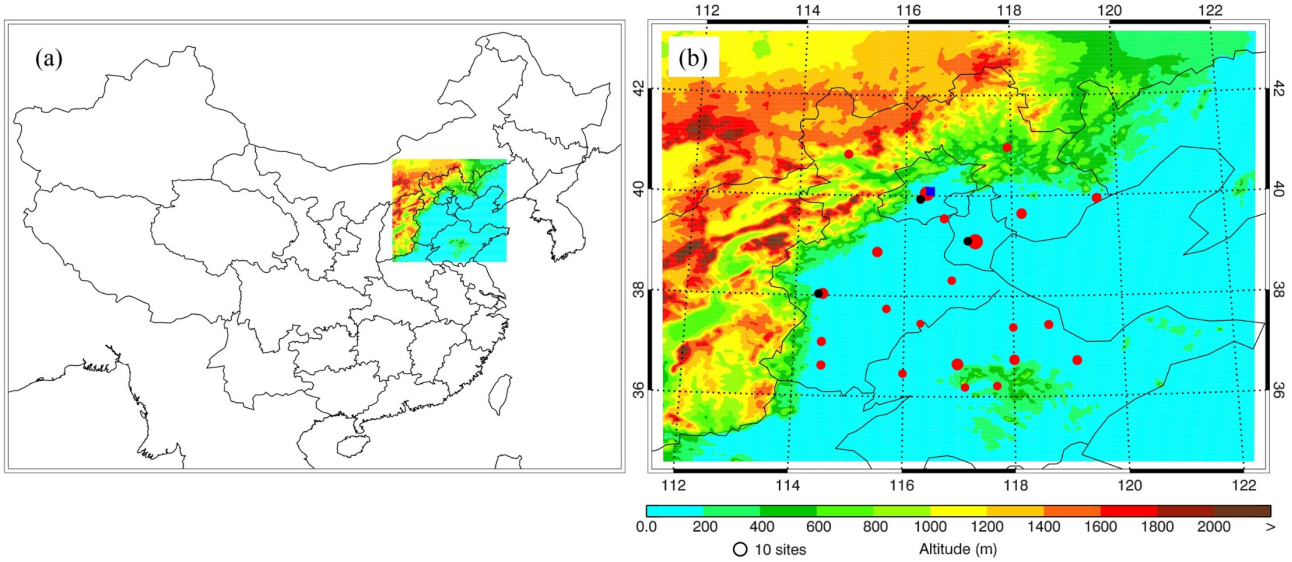

Figure 1 (a) Map showing the location of Beijing-Tianjin-Hebei and (b) WRF-Chem model simulation domain with topography. In (b), the filled red circles represent centers of cities with ambient monitoring site and the size of the circle denotes the number of ambient monitoring sites of cities. The filled blue rectangle denotes the deployment location of the HR-ToF-AMS in Beijing. The three filled black circles represent the location of the meteorological observation stations in Beijing, Tianjin, and Shijiazhuang, respectively.

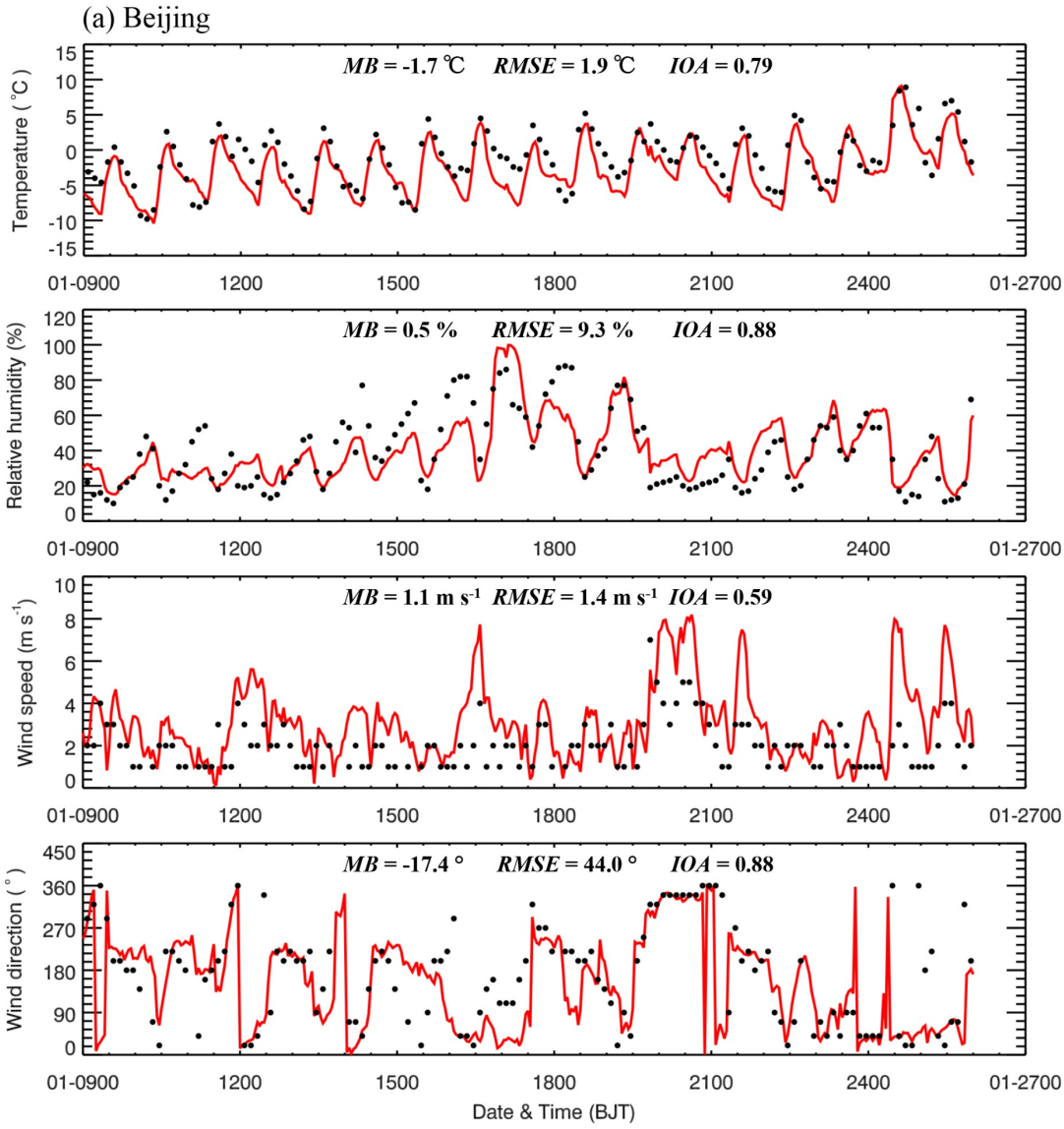

Figure 2 Comparisons of observed (black dots) and simulated (solid red lines) diurnal profiles of near-surface temperature, relative humidity (RH), wind speed, and wind direction at meteorological sites in (a) Beijing, (b) Tianjin, and (c) Shijiazhuang from 9 to 25 January 2014.

(b) Tianjin

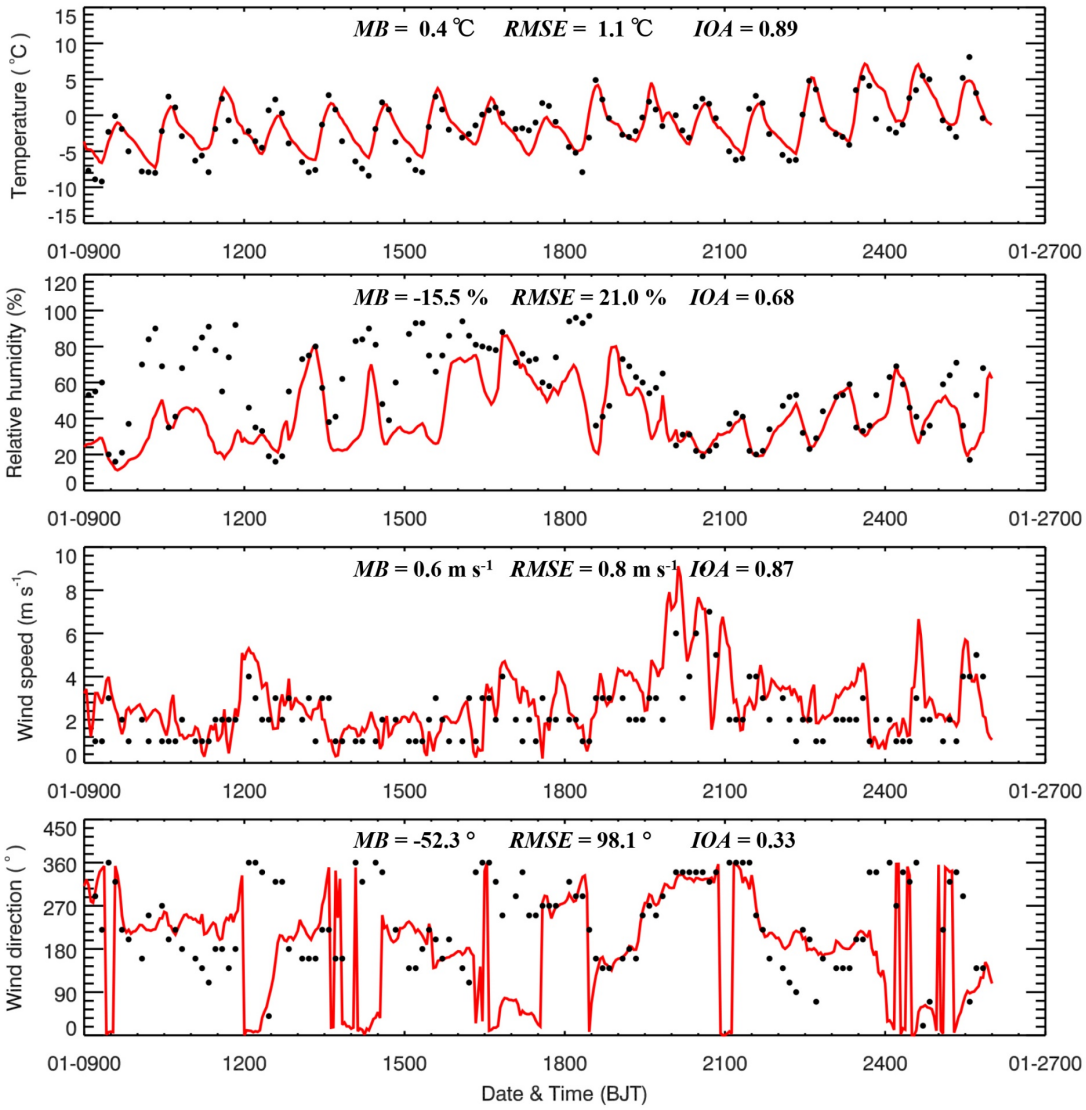

Figure 2 continued.

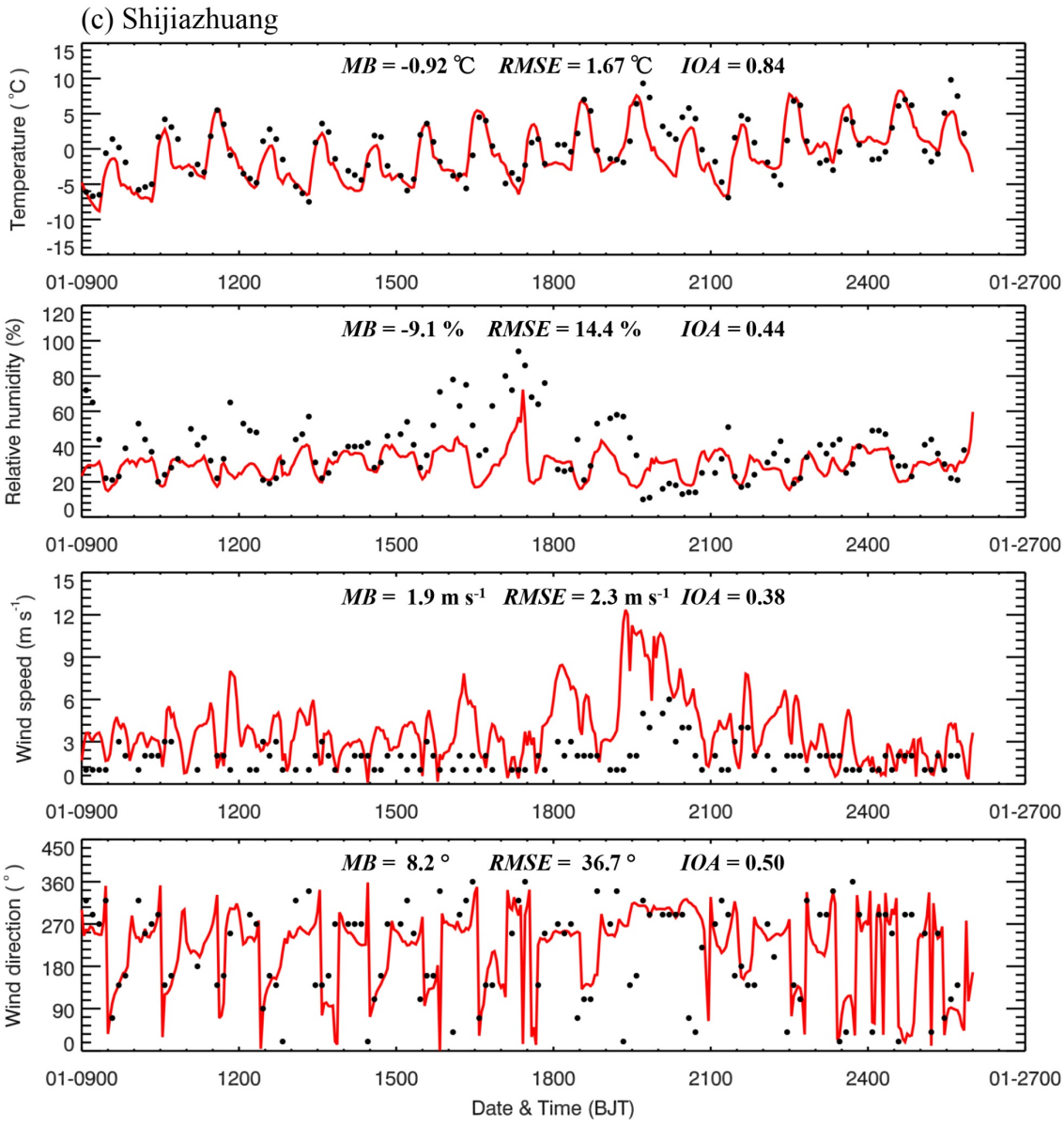

Figure 2 continued.

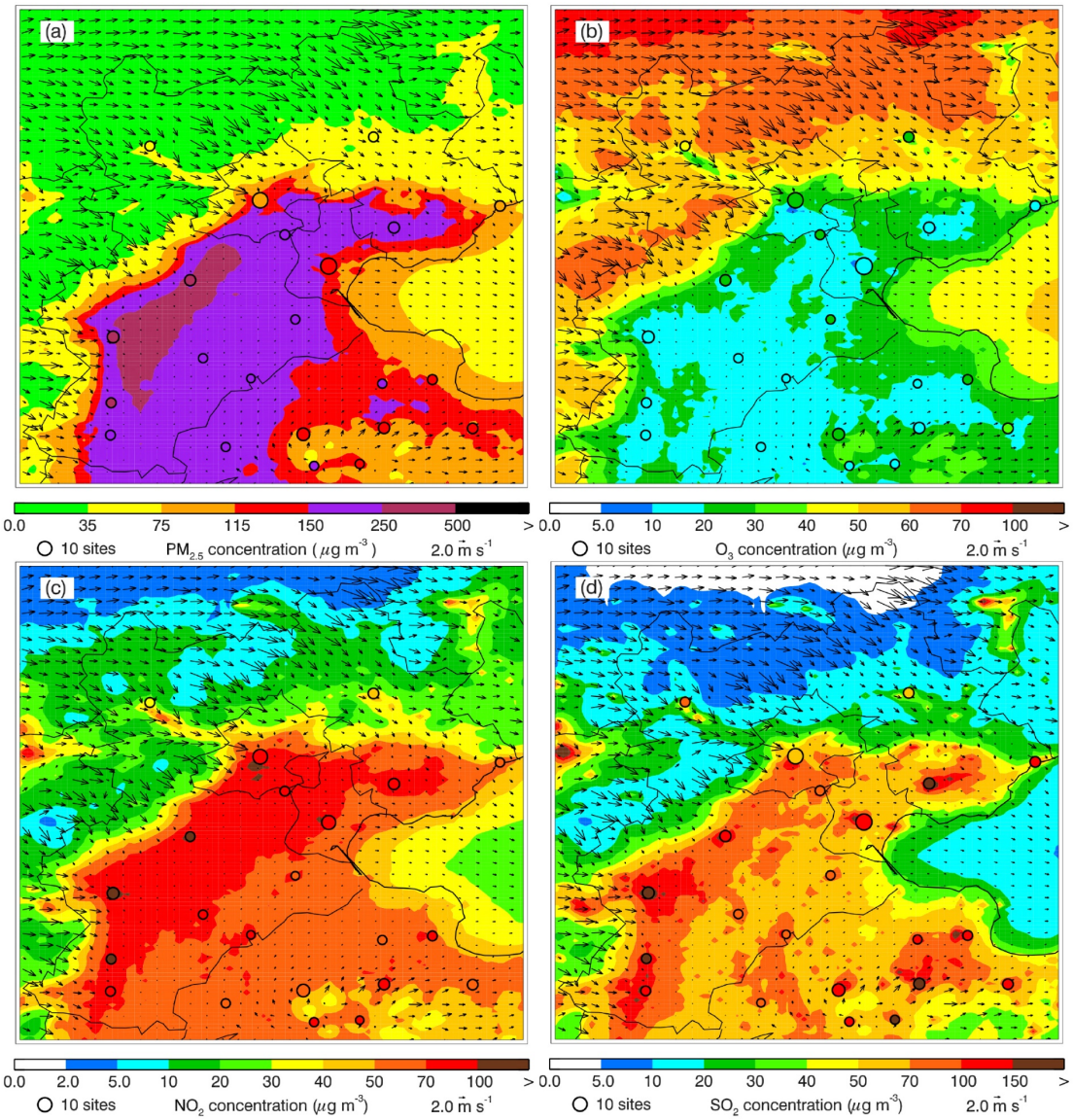

Figure 3 Pattern comparisons of simulated (color counters) vs. observed (colored circles) near-surface mass concentrations of (a) $PM_{2.5}$, (b) O_3, (c) NO_2, and (d) SO_2 averaged from 9 to 25 January 2014. The black arrows indicate simulated surface winds.

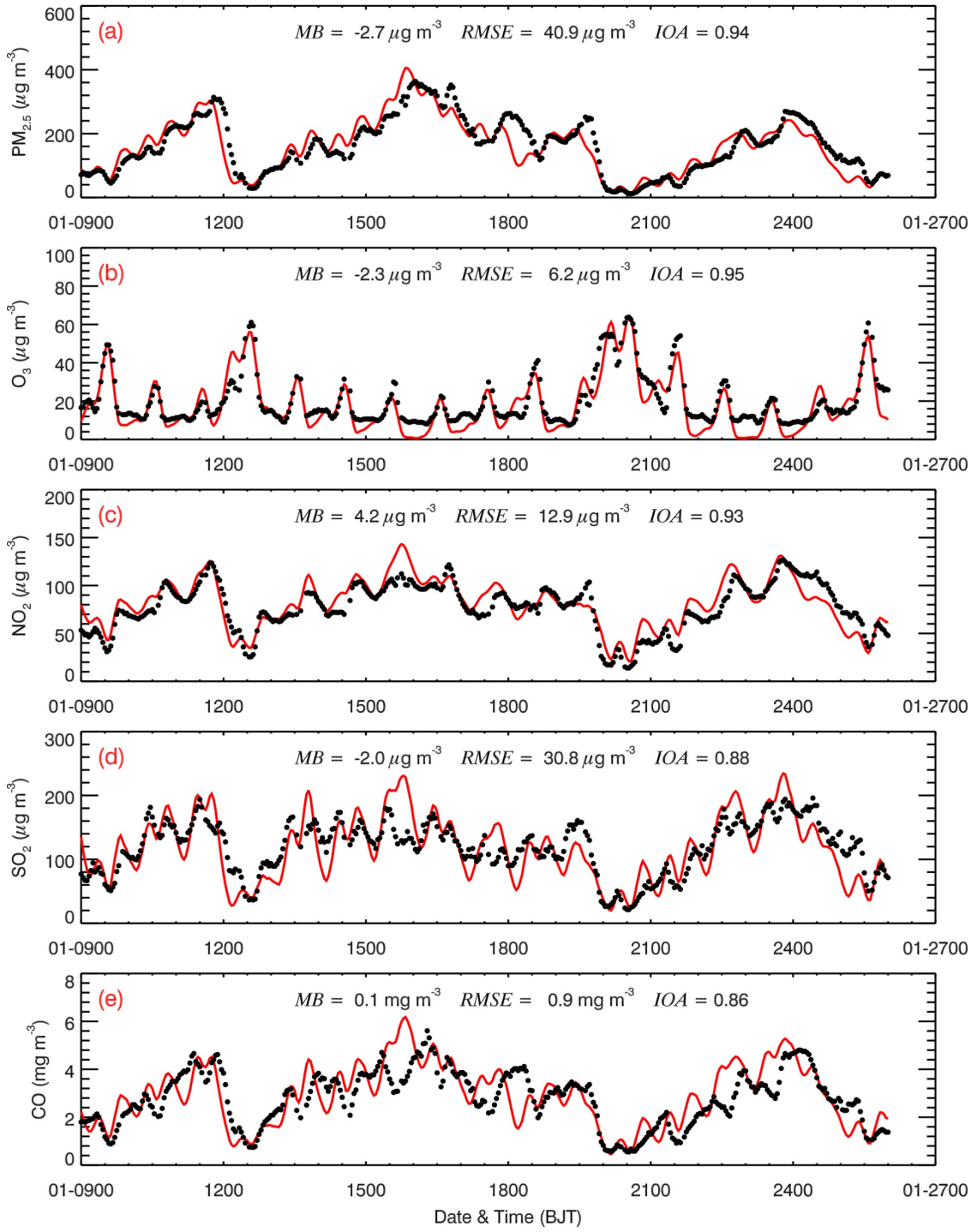

Figure 4 Comparisons of observed (black dots) and simulated (solid red lines) diurnal profiles of near-surface hourly mass concentrations of (a) $PM_{2.5}$, (b) O_3, (c) NO_2, (d) SO_2, and (d) CO averaged at monitoring sites in BTH from 9 to 25 January 2014.

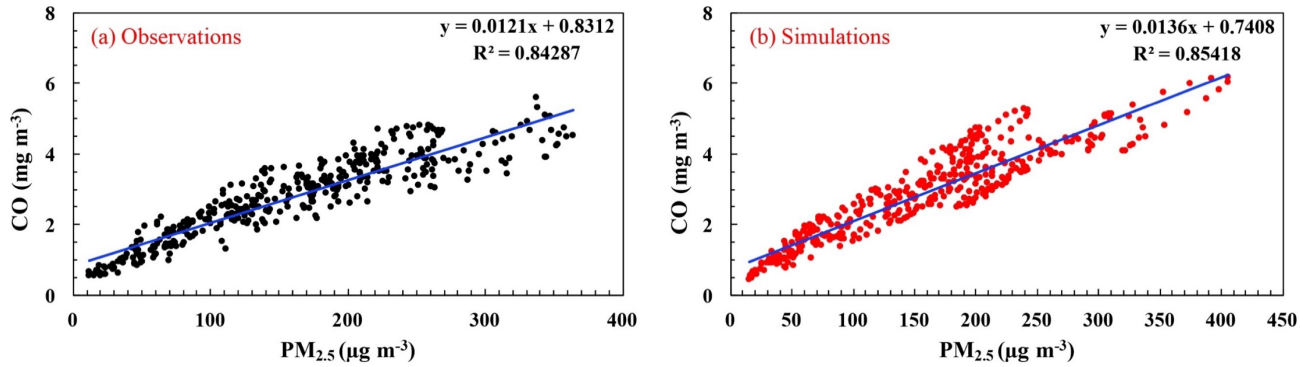

Figure 5 Scatter plots of the (a) observed and (b) simulated $PM_{2.5}$ with CO mass concentrations averaged over all ambient monitoring sites in BTH from 9 to 25 January 2014.

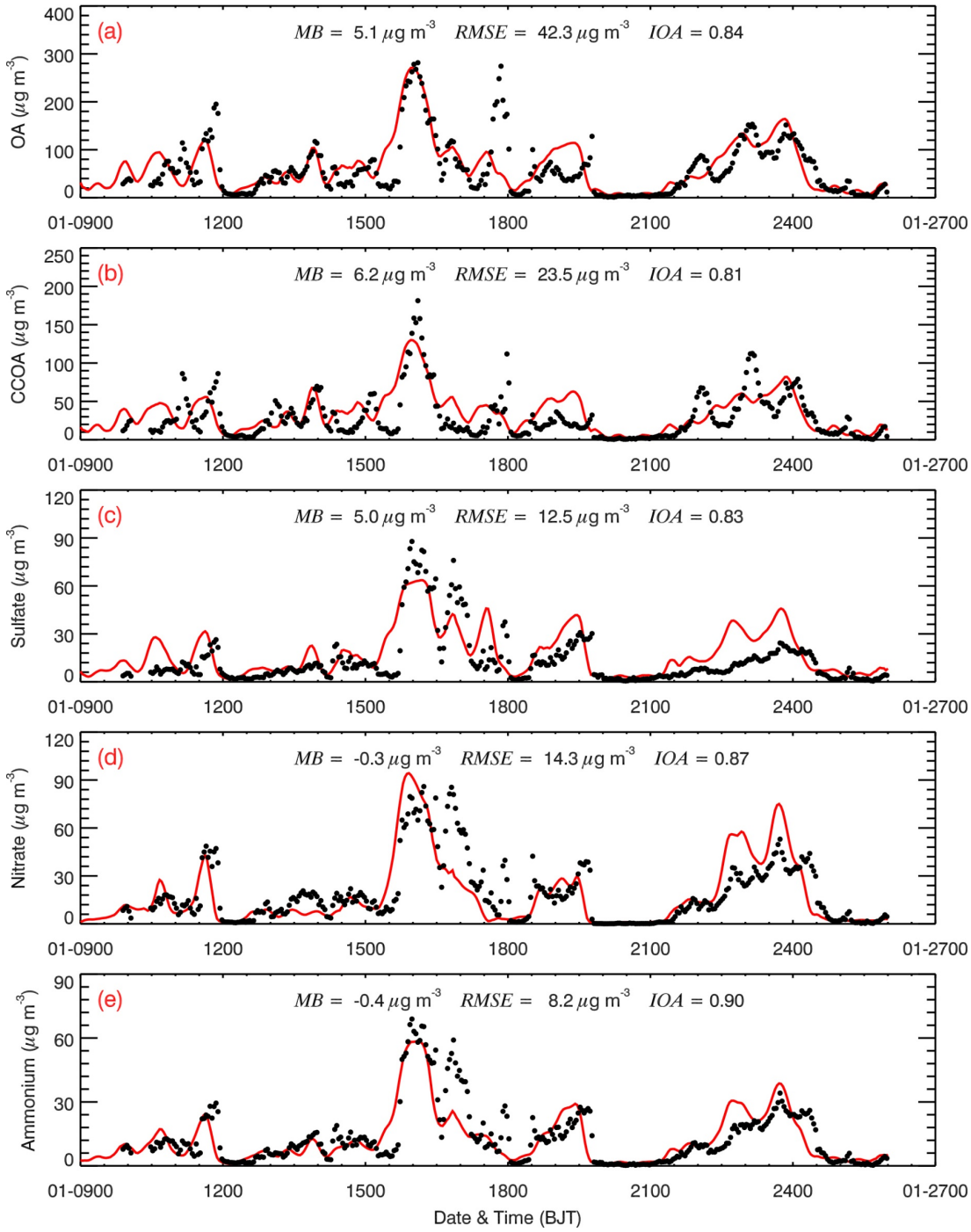

Figure 6 Comparisons of measured (black dots) and simulated (solid red lines) diurnal profiles of (a) organic aerosol (OA), (b) coal combustion organic aerosol (CCOA), (c) sulfate, (d) nitrate, and (e) ammonium in Beijing from 9 to 25 January 2014.

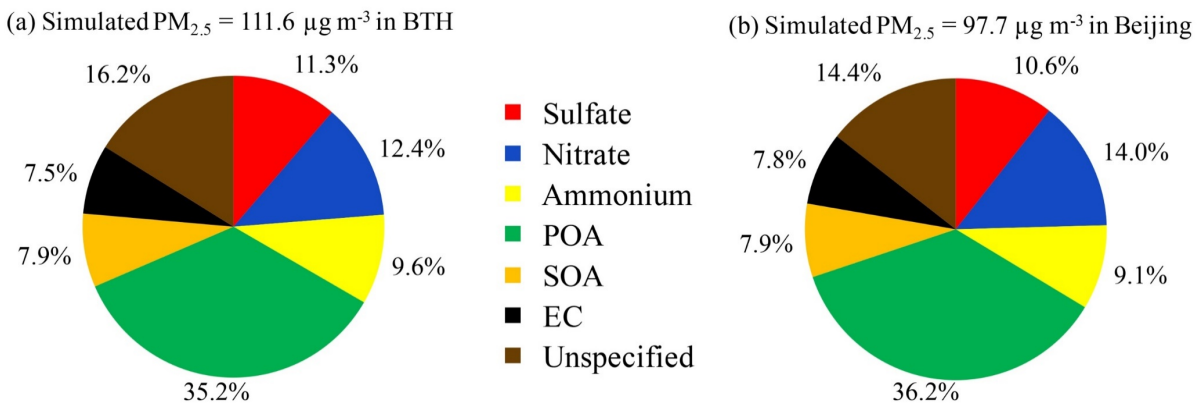

Figure 7 Chemical composition of $PM_{2.5}$ averaged from 9 to 25 January 2014 in (a) BTH and (b) Beijing.

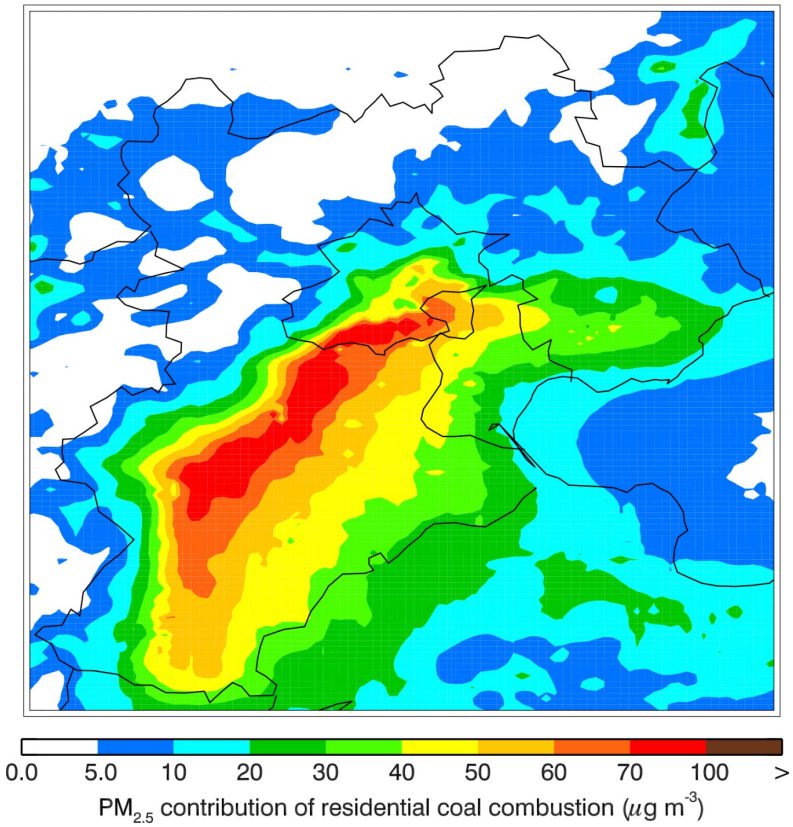

Figure 8 Spatial distribution of the average contribution of the RCC emission in BTH to $PM_{2.5}$ mass concentrations from 9 to 25 January 2014.

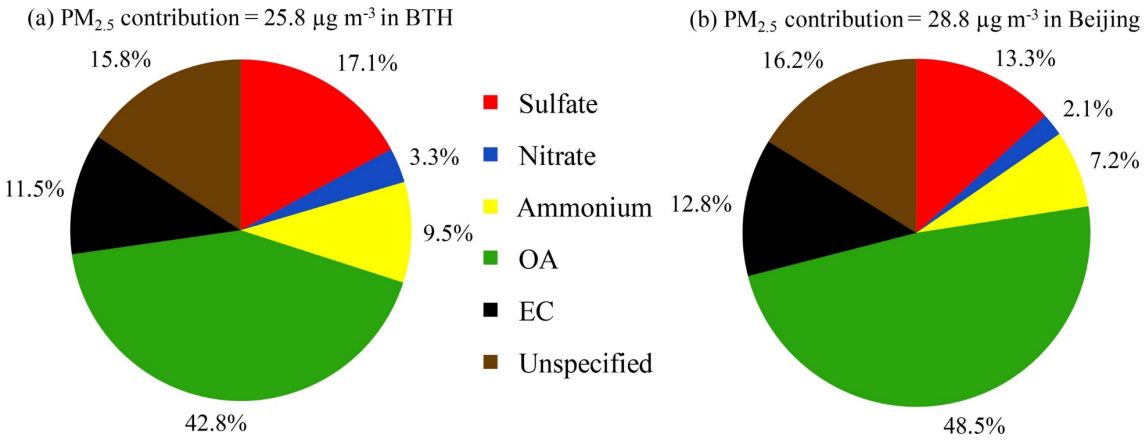

Figure 9 Chemical composition of $PM_{2.5}$ from the RCC emission in BTH averaged from 9 to 25 January 2014 in (a) BTH and (b) Beijing.

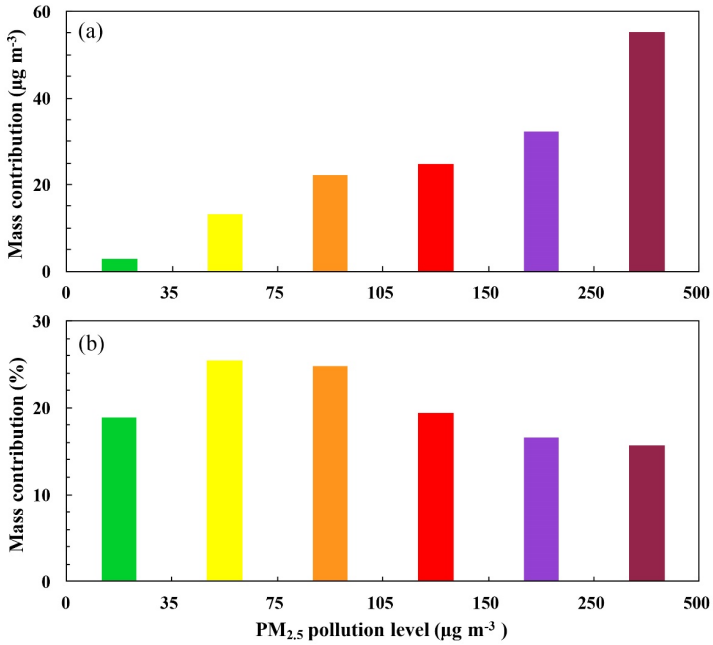

Figure 10 Average contributions of the RCC emission in Beijing to the local $PM_{2.5}$ mass concentrations under different haze pollution levels from 9 to 25 January 2014. The green, yellow, orange, red, purple, and dark red color bar in the plots represents excellent, good, slightly polluted, moderately polluted, heavily polluted, and severely polluted levels of air quality, respectively.